On the Similarity Functions A, B and C of the Planetary Boundary Layer

TETSUJI YAMADA

Geophysical Fluid Dynamics Program,[1] Princeton University, Princeton, N. J. 08540

(Manuscript received 21 July 1975, in revised form 19 January 1976)

ABSTRACT

The similarity functions A, B and C are computed based on the various scales previously proposed for wind, temperature and height in the planetary boundary layer. The vertically averaged geostrophic wind recently proposed by Arya and Wyngaard is found to be a better choice as a wind scale for the Wangara experiment than a local wind at a specified height. A similar conclusion is drawn for the temperature scale. As for the height scale the similarity functions A, B and C scaled by the height of the surface inversion layer during the nighttime resulted in relatively less scatter than those scaled by $u_*/|f|$.

Nomograms for the geostrophic drag and the heat transfer coefficients are presented by utilizing the approximate expressions for A, B and C deduced from the Wangara data. Agreement between the values predicted and those deduced from the data appears to support the appropriateness of the present choice of the scales originally suggested by Arya and Wyngaard.

1. Introduction

Recently a considerable number of discussions have appeared on the geostrophic drag and heat transfer coefficients for the atmospheric boundary layer. This is partly due to a practical demand for a simple method to determine the surface turbulence fluxes in numerical models (Clarke, 1970a). But it is largely due to the fact that more and more observed data have become available with which theories can be tested. Although some success has been achieved with similarity theories under idealized atmospheric conditions, i.e., stationary, horizontally homogeneous, and neutrally stratified (Csanady, 1967; Blackadar and Tennekes, 1968; Brown, 1974), their counterparts under more realistic conditions have not been fully validated with observed data (Kazanski and Monin, 1960; Zilitinkevich *et al.*, 1967; Gill, 1968; Zilitinkevich and Chalikov, 1968; Clarke, 1970b; Clarke and Hess, 1974; Melgarejo and Deardorff, 1974, 1975; Arya, 1975; Zilitinkevich, 1975).

The universal functions A, B and C which are computed from observed data differ for individual investigators and exhibit a great degree of scatter. Arya (1975), for example, recently reanalyzed the works by Zilitinkevich and Chalikov (1968) and Clarke (1970b) and successfully reduced the large difference which had existed between their results by applying to both cases the same format and an improved method to obtain the surface heat and momentum fluxes. Although some improvements were made, the similarity functions A, B and C obtained by Arya still contained considerable variations especially for values under stable conditions.

It is the purpose of the present study to demonstrate how the scatter in the similarity functions computed from observed data would be reduced if the scales for the wind, temperature and height are appropriately chosen.

[1] Support provided through Geophysical Fluid Dynamics Laboratory/NOAA under Grant 04-3-022-33.

2. Formulation of the problem

According to the similarity theory it is assumed that if a variable (wind, temperature, etc.) is appropriately scaled then its profile follows a universal function whose form, in general, must be determined empirically.

For the flow far away from the surface we assume that

$$\frac{\mathbf{V}-\hat{\mathbf{V}}}{u_*}\equiv\mathbf{F}\left(\frac{z}{h},\frac{h}{L}\right)\equiv\mathbf{t}\cdot F_u\left(\frac{z}{h},\frac{h}{L}\right)+\mathbf{n}\cdot F_v\left(\frac{z}{h},\frac{h}{L}\right)\mathrm{sign}f, \quad (1a,b)$$

$$\frac{\Theta_v-\hat{\Theta}_v}{T_*}=F_{\Theta_v}\left(\frac{z}{h},\frac{h}{L}\right), \quad (1c)$$

where $\mathbf{t}$ and $\mathbf{n}$, respectively, are the unit vectors tangential and normal to the surface wind direction; $\hat{\mathbf{V}}$ is the wind scale and $\hat{\Theta}_v$ the temperature scale; $u_*(T_*)$ the friction velocity (temperature); and F_u,

F_v, F_{Θ_v} the universal outer (profile) functions for (U,V,Θ_v). (The rest of the symbols are defined in Appendix A.)

For the flow in the surface layer we assume that

$$\frac{\mathbf{V}}{u_*}=\frac{\mathbf{t}}{k}\left[\ln\left(\frac{z}{z_0}\right)-\psi_m\left(\frac{z}{L}\right)\right], \tag{2a,b}$$

$$\frac{\Theta_v-\Theta_{v0}}{T_*}=\frac{\mathrm{Pr}_0}{k}\left[\ln\left(\frac{z}{z_0}\right)-\psi_h\left(\frac{z}{L}\right)\right], \tag{2c}$$

where ψ_m and ψ_h are the stability functions for U and Θ_v, respectively; Θ_{v0} is the virtual potential temperature at $z=z_0$; and Pr_0 is the turbulent Prandtl number at the neutral stability whose numerical value is assumed to be 0.74 according to Businger *et al.* (1971).

It is commonly assumed that there exists a layer where both (1) and (2) are simultaneously satisfied. Following the procedure described by Hess (1973), we obtain the following relation by matching (1a,b) and (2a,b):

$$\frac{\mathbf{t}}{k}\ln\left(\frac{h}{z_0}\right)-\frac{\hat{\mathbf{V}}}{u_*}=\frac{\mathbf{E}}{k}\left(\frac{h}{L}\right). \tag{3}$$

Substitution of $\mathbf{E}(h/L)=A(h/L)\cdot\mathbf{t}+B(h/L)\cdot\mathbf{n}$ into (3) gives

$$A(h/L)=\ln(h/z_0)-k\hat{U}/u_*, \tag{4a}$$

$$B(h/L)=-\frac{k\hat{V}}{u_*}\,\mathrm{sign}f. \tag{4b}$$

In a similar fashion matching (1c) and (2c) gives

$$C(h/L)=\ln(h/z_0)-(k/\mathrm{Pr}_0)(\hat{\Theta}_v-\Theta_{v0})/T_*. \tag{4c}$$

The functions A, B (notations for A and B are chosen differently by different authors) and C in (4a,b,c) are the similarity functions which shall be determined later from observed data.

The geostrophic drag coefficient is obtained from (4a,b) as

$$C_D\equiv\frac{u_*}{|\hat{\mathbf{V}}|}=k\{[\ln(h/z_0)-A]^2+B^2\}^{-\frac{1}{2}}, \tag{5a}$$

where $|\hat{\mathbf{V}}|\equiv[\hat{U}^2+\hat{V}^2]^{\frac{1}{2}}$. The heat transfer coefficient from (4c) is

$$C_H\equiv\frac{T_*}{\hat{\Theta}_v-\Theta_{v0}}=\frac{k}{\mathrm{Pr}_0}[\ln(h/z_0)-C]^{-1}. \tag{5b}$$

The angle between the direction of the surface wind and that of the wind vector, $\hat{\mathbf{V}}=\hat{U}\cdot\mathbf{t}+\hat{V}\cdot\mathbf{n}$, may be obtained from (4b) as

$$\sin\theta=\frac{-u_*}{k|\hat{\mathbf{V}}|}B\cdot\mathrm{sign}f. \tag{6}$$

For the barotropic atmosphere the appropriate scales for wind and height are

$$\hat{\mathbf{V}}=\mathbf{V}_g, \tag{7a,b}$$

$$h=\alpha\frac{u_*}{|f|},\quad \alpha\approx 0.30, \tag{7c}$$[2]

where $\mathbf{V}_g\equiv U_g\cdot\mathbf{t}+V_g\cdot\mathbf{n}$ is the geostrophic wind vector. The scales in (7a,b,c) are consistent with the mean equation of motion as shown for example by Blackadar and Tennekes (1968). In the real atmosphere, however, the geostrophic wind is not constant with height due to the thermal wind effect. Furthermore, as noted by Clarke and Hess (1974), the accuracy in measuring the horizontal pressure gradients (which are necessary to determine the geostrophic wind) is limited by the sensitivity of the pressure sensors presently available. On the other hand, wind speed can be measured more accurately. Therefore, for example, the wind at the height of the surface inversion layer during the nighttime and the wind at the height of the mixed layer during the daytime (Melgarejo and Deardorff, 1974), or wind at the height of 0.15 $u_*/|f|$ above the surface (Clarke and Hess, 1974), or the maximum wind (Clarke, 1970b) have been utilized as the velocity scales in place of the geostrophic wind. The winds determined in these ways are, in general, subgeostrophic during the daytime and supergeostrophic during the nighttime (Clarke and Hess, 1974).

Similarly, controversial arguments on the height scale have been reported. Clarke and Hess (1973) gave one example which indicated that $u_*/|f|$ as the height scale was a slightly better choice than the height of the inversion layer proposed by Deardorff (1972) and Wyngaard *et al.* (1974), or the Obukhov stability scale by Csanady (1972). The findings by Melgarejo and Deardorff (1974, 1975), however, appeared to indicate that the similarity functions A, B and C scaled by the height of the surface inversion layer under stable conditions showed relatively less scatter than those scaled by $u_*/|f|$.

3. Method of evaluating A, B and C

Recently Arya and Wyngaard (1975) suggested utilization of a vertically averaged geostrophic wind as a wind scale for the convective planetary boundary layer and examined the effects of baroclinicity on the similarity functions A and B. More specifically, the functions A and B, which are based on the vertically averaged geostrophic wind, were decomposed into two components—one based on the surface geostrophic wind and another due to the baroclinicity. Therefore,

[2] If $0.3\,u_*/|f|>z_i$, where z_i is the height of the inversion layer, $h=z_i$ may be more appropriate. For the Wangara data set utilized here, however, we found that in most strongly unstable cases $0.3\,u_*/|f|<z_i$ as seen from Fig. 11.

the latter term should vanish if the atmosphere is in barotropic balance. Although Arya and Wyngaard convincingly demonstrated the effects of baroclinicity on A and B when the geostrophic wind profile was assumed to vary linearly with height, the usefulness of their approach in a practical application was unclear. In the present paper, on the other hand, we seek a direct way to determine the similarity functions A and B which are based on the vertically averaged geostrophic wind. Then we shall compare the drag coefficients predicted by the similarity functions A and B with the values deduced from the Wangara data (Clarke *et al.*, 1971). Similar analysis will be applied for the heat transfer coefficient and the surface wind angle.

Although Arya and Wyngaard originally suggested usage of the vertically averaged geostrophic wind only in the convective planetary boundary layer, we extend the vertical averaging procedure to the virtual potential temperature and apply it both under stable and unstable conditions. We utilize the following scales for the wind and virtual potential temperature:

$$\hat{\mathbf{V}}=\langle \mathbf{V}_g\rangle \equiv \frac{1}{h}\int_{z_0}^{h}\mathbf{V}_g dz, \tag{8a,b}$$

$$\hat{\Theta}_v=\langle \Theta_v\rangle \equiv \frac{1}{h}\int_{z_0}^{h}\Theta_v dz, \tag{8c}$$

where the height scale h is taken as the height where the turbulence vanishes which occurs near the top of the mixed layer during daytime and near the height of the surface inversion layer during nighttime. If the atmosphere is barotropic, i.e., $\langle U_g\rangle = U_{g0}$ and $\langle V_g\rangle = V_{g0}$, then a conventional geostrophic departure relation is recovered. Since the geostrophic wind profiles are not, in general, available we infer $\langle U_g\rangle$ and $\langle V_g\rangle$ from the mean equations of motion:

$$\mathrm{sign}f\cdot\frac{\partial}{\partial z}(-\overline{uw})=-|f|(V-V_g), \tag{9a}$$

$$\mathrm{sign}f\cdot\frac{\partial}{\partial x}(-\overline{vw})=|f|(U-U_g), \tag{9b}$$

where stationary, horizontally homogeneous flow is assumed. Integrating (9a,b) from z_0 to h we obtain

$$\langle U_g\rangle=\langle U\rangle, \tag{10a}$$

$$\langle V_g\rangle=\langle V\rangle-\frac{u_*^2}{|f|h}\mathrm{sign}f, \tag{10b}$$

where

$$\langle\eta\rangle\equiv\frac{1}{h}\int_{z_0}^{h}\eta dz,\quad \eta=(U,V,U_g,V_g).$$

Boundary conditions utilized for the integration to obtain (10a, b) are

$$-\overline{uw}(z_0)=u_*^2,\quad -\overline{vw}(z_0)=-\overline{uw}(h)=-\overline{vw}(h)=0. \tag{10c}$$

Substitution of (10a,b) into (4a,b) yields

$$A(h/L)=\ln(h/z_0)-\frac{k\langle U\rangle}{u_*}, \tag{11a}$$

$$B(h/L)=\frac{ku_*}{|f|h}-\frac{k\langle V\rangle}{u_*}\mathrm{sign}f. \tag{11b}$$

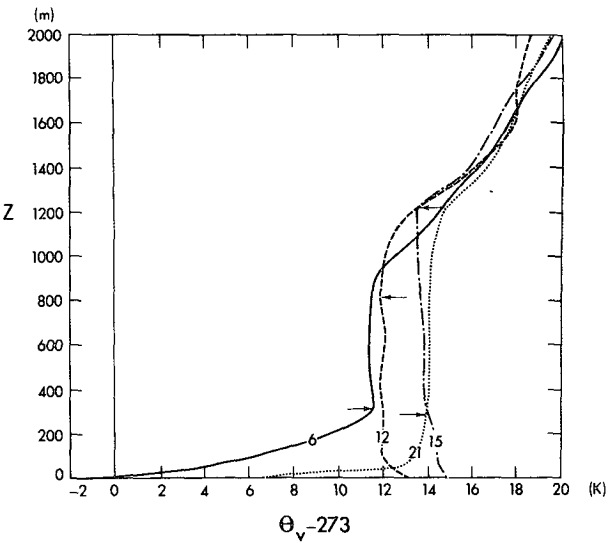

FIG. 1. Observed virtual potential temperature profiles and height scales h indicated by arrows. Numerical values on the profiles indicate times on Day 33 of the Wangara experiment.

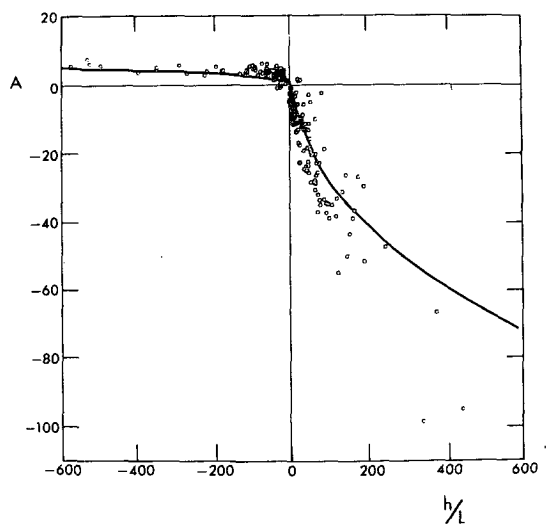

FIG. 2. Similarity function A vs h/L. Vertically averaged geostrophic wind is utilized as a wind scale.

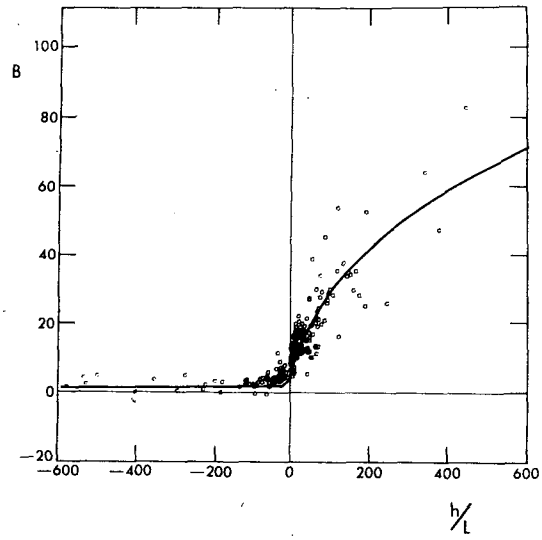

FIG. 3. As in Fig. 2 except for B.

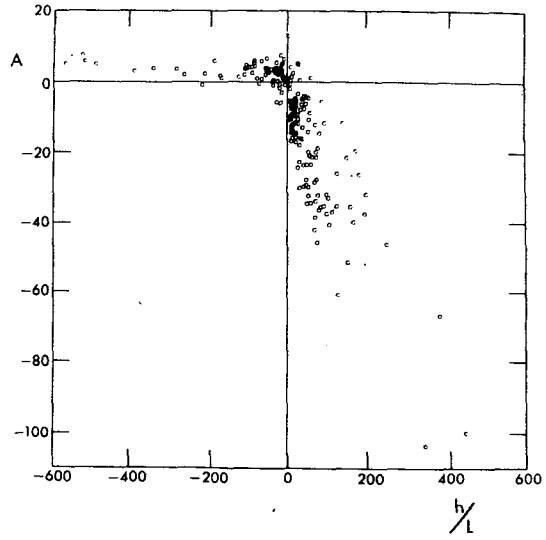

FIG. 5. Similarly function A vs h/L. A local wind at $z=h$ is utilized as a wind scale.

Substituting (8c) into (4c) we have

$$C(h/L)=\ln(h/z_0)-\frac{k}{\mathrm{Pr}_0}\frac{\langle\Theta_v\rangle-\Theta_{v0}}{T_*}. \qquad (11c)$$

The similarity functions A, B and C will be evaluated in the following section utilizing observed data and (11a,b,c).

4. Results and discussion

a. Similarity functions A, B and C

The Wangara atmospheric boundary layer data observed at Hay, Australia (Clarke *et al.*, 1971), are utilized to examine the scales discussed in the previous section. A complete description of the Wangara experiment is given by Clarke *et al.* from which we extract the information necessary to the present study. First the virtual potential temperature is computed from

$$\Theta_v\equiv(T+\gamma_d z)(1+0.61R),$$

where T is absolute temperature (K), R the mixing ratio of water vapor, and γ_d the dry adiabatic lapse rate [10 K (1000 m)$^{-1}$]. Temperature and mixing ratio are available every 3 h at every 50 m interval for the first 1000 m above the surface then at every 100 m interval up to 2000 m. The height scale h is determined from the vertical profiles of the virtual potential temperature as illustrated in Fig. 1.[3] Then the height scales between the observed hours (every 3 h) may be obtained from the curve fitted to the h vs time diagram determined above. Once h is determined, the temperature scale may be computed from (8c). Similarly, wind scales (10a,b) are obtained by integrating (from z_0 to h) the wind components U and V which are measured every hour at the same heights as for temperature.

In order to compute the friction velocity and surface heat flux the surface wind at 0.5 m and tempera-

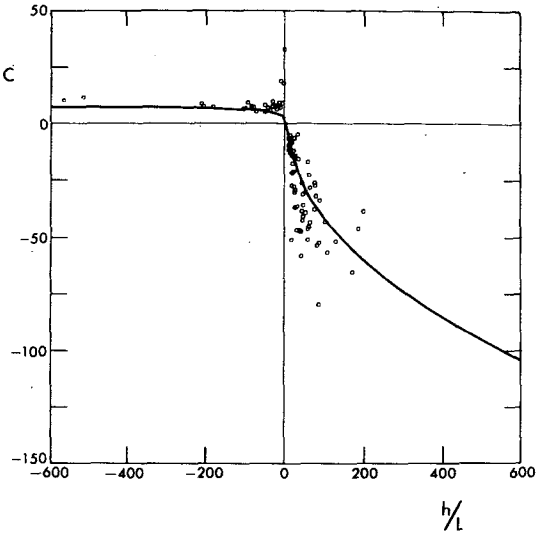

FIG. 4. Similarity function C vs h/L. Vertically averaged virtual potential temperature is utilized as a temperature scale.

[3] Boundary conditions for the momentum fluxes at h given by (10c) may not be satisfied in the convective boundary layer due to the entrainment near h (Deardorff, 1973). Therefore h determined from Fig. 1 under unstable conditions may underestimate a true h value which should satisfy (10c). Exact difference between h defined by (10c) and one determined from Fig. 1 cannot be estimated from the Wangara data but an approximate magnitude may be in the order of 100–200 m at most according to the numerical simulation reported by Deardorff (1973). Error due to this much difference in h on A and B [(11a) and (11b)] are found to be small due to the fact that h appears within the logarithmic argument for A. Also A and B are almost independent of stability under unstable conditions as seen from Figs. 2 and 3.

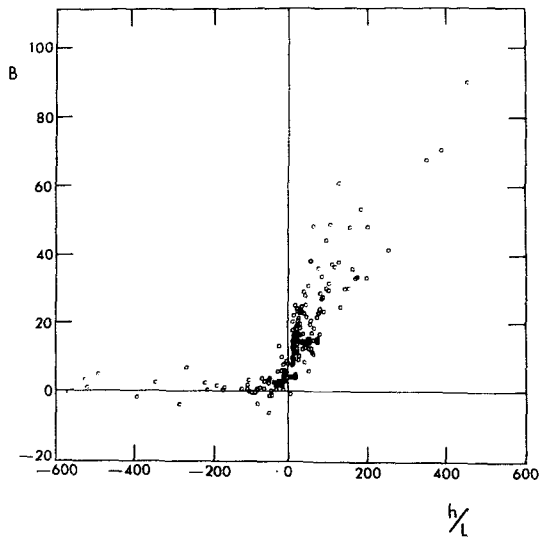

FIG. 6. As in Fig. 5 except for B.

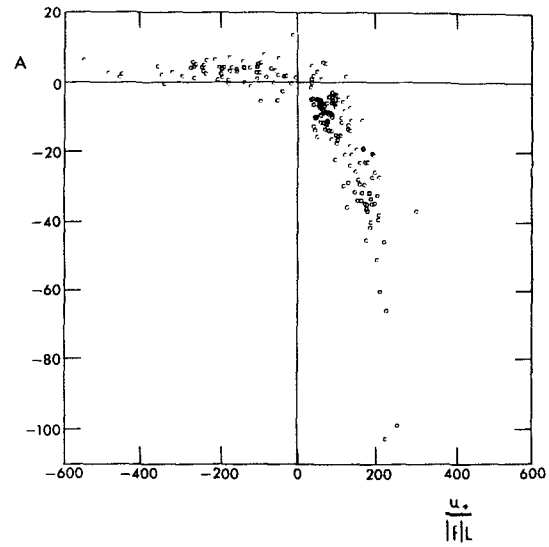

FIG. 8. Similarity function A vs $u_*/|f|L$. A local wind at $z=h$ is utilized as a wind scale.

ture difference between 1 and 4 m at station 5 are utilized. Empirical expressions for the wind and temperature profiles deduced by Businger *et al.* (1971) from the surface layer measurements are adopted. Friction velocity and surface heat flux are obtained by a similar procedure as described by Paulson (1970) but appropriate equations are solved iteratively rather than using a relation $\mathrm{Ri}=L$ under unstable conditions, where L is the Obukhov length. A simpler procedure is utilized under stable conditions where L is given as a solution of a quadratic equation. A reviewer of this paper pointed out that the stability computations should not be based on the temperature difference between 1 and 2 m because of the instrumental error (Hicks, 1975). For further details on this matter, readers are referred to the discussions in Appendix B. The roughness height $z_0=0.12$ cm and Coriolis parameter $f=-0.826\times10^{-4}$ s^{-1} (latitude 34°30′ S) are utilized.

The similarity functions A, B and C are computed from (11a,b,c) with values obtained above for the surface fluxes (see Appendix B), the vertically averaged wind and temperature scales, and the height scale. A total of 199 runs (hours) is analyzed for A and B mainly for the periods from days 11 through 14 and days 31 through 38 excluding the transitional hours in the morning (0700 to 0900) and in the evening (1600 to 2000).[4] In addition, most of the data utilized

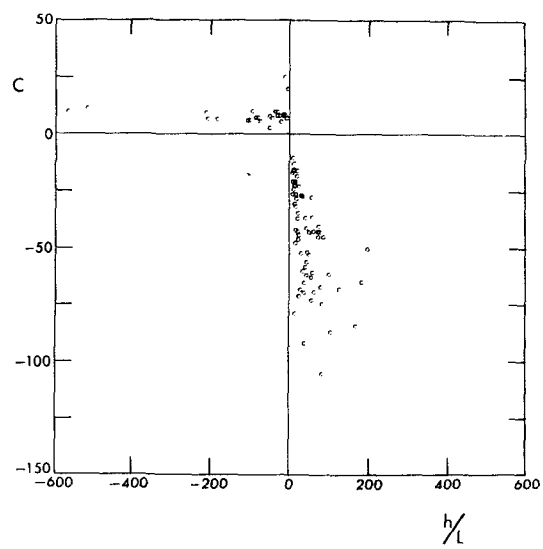

FIG. 7. As in Fig. 5 except for C. A local virtual potential temperature at $z=h$ is utilized as a temperature scale.

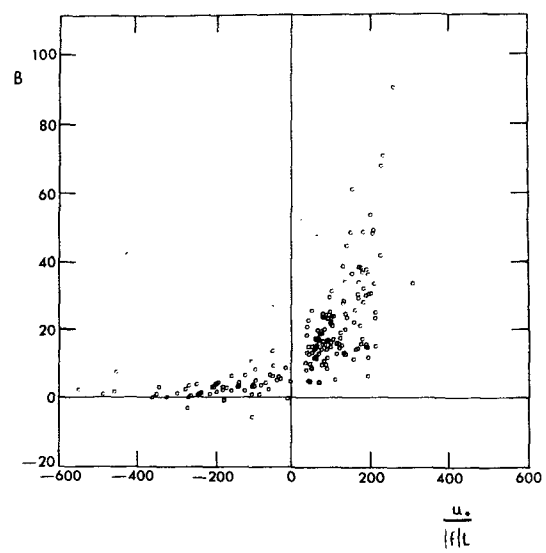

FIG. 9. As in Fig. 8 except for B.

[4] Although approximately 500 runs of the data are available for wind (excluding the transitional hours), about one-third

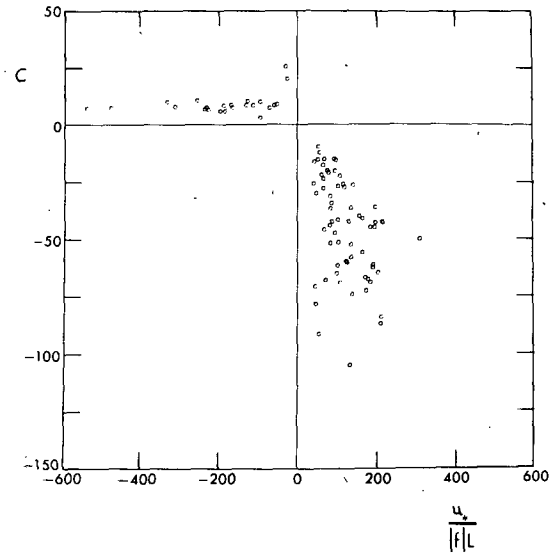

FIG. 10. As in Fig. 8 except for C. A local virtual potential temperature at $z=h$ is utilized as a temperature scale.

by Melgarejo and Deardorff (1974) are included. For C a total of 92 runs is presented.

Although familiar scatter in the similarity functions A, B and C (Figs. 2, 3, 4) is seen, especially in C under stable conditions, the present results seem to indicate considerable improvement over those previously reported (Clarke, 1970b; Melgarejo and Deardorff, 1975; Arya, 1975). No statistical analysis on the variations is conducted due to the small sampling numbers at any h/L value but a comparison of A and B under

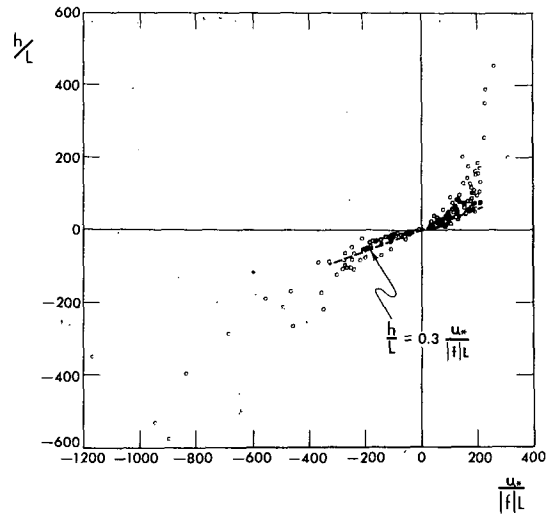

FIG. 11. Dimensionless height scales h/L vs $u_*/|f|L$.

must be excluded due to large-scale disturbances (fronts passed the observational site approximately every 10 days and strong disturbances remained for a couple of days after such passages). It appears that the 199 runs analyzed here cover a fairly wide range of stability conditions as seen from figures presented later.

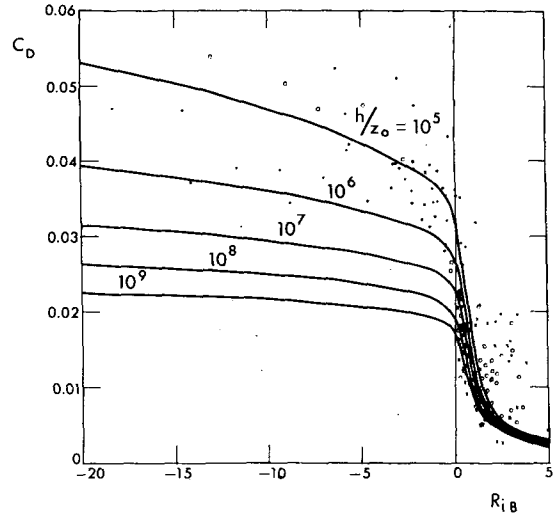

FIG. 12. Drag coefficient C_D as a function of the bulk Richardson number Ri_B: (○) $10^5 \leqslant h/z_0 < 10^6$; (×) $10^6 \leqslant h/z_0 < 10^7$; (□) $10^7 \leqslant h/z_0 < 10^8$; (*) $10^8 \leqslant h/z_0 < 10^9$; (+) $10^9 \leqslant h/z_0 < 10^{10}$. Solid lines are predictions by (5a) where A and B are given by (13a,b), (14a,b), (16) and (17).

unstable conditions with those by Clarke and Hess (1974) seems to indicate that the present results are comparable with theirs.

In order to demonstrate the importance of the scales the same data set was reanalyzed based on the wind and temperature at h as suggested by Melgarejo and Deardorff (1974) in place of the vertically averaged wind and temperature. The resultant A, B and C are shown in Figs. 5, 6 and 7, respectively. The general appearances are similar to those in Figs. 2, 3 and 4, but the degree of scatter is noticeably increased under both stable and unstable conditions.

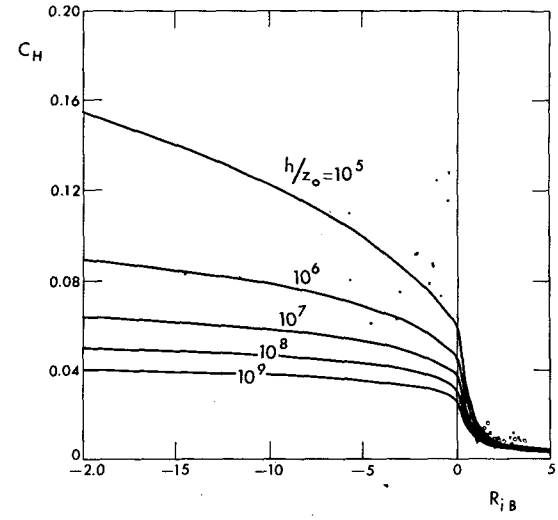

FIG. 13. As in Fig. 12 except for heat transfer coefficient C_H Solid lines are predictions by (5b) where C is given by (15a,b) and (18).

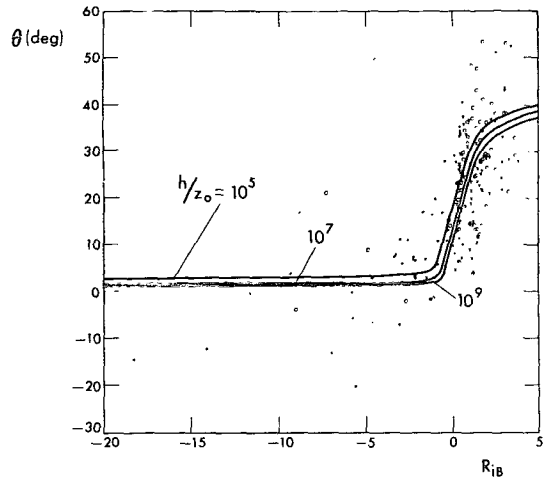

FIG. 14. As in Fig. 12 except for angle θ. Solid lines are predictions by (6) where B is given by (14a,b) and (17).

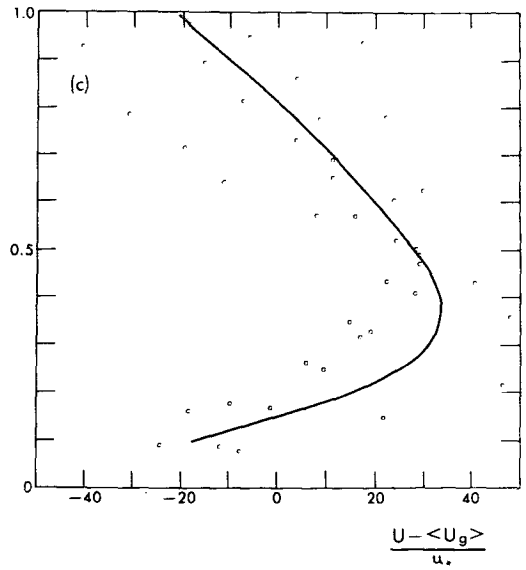

FIG. 15. Wind defect $(U-\langle U_g\rangle)/u_*$ (abscissa) vs z/h (ordinate): (a) $-150\leqslant h/L\leqslant -120$; (b) $0\leqslant h/L\leqslant 30$; (c) $180\leqslant h/L\leqslant 210$.

In additional analysis a more conventional height scale of $u_*/|f|$ was adopted but the wind and temperature at h were again utilized as the wind and temperature scales. The resultant A, B and C are shown in Figs. 8, 9 and 10, respectively. Clearly, more scatter in A, B and C is depicted in Figs. 8, 9 and 10 than in Figs. 5, 6 and 7.

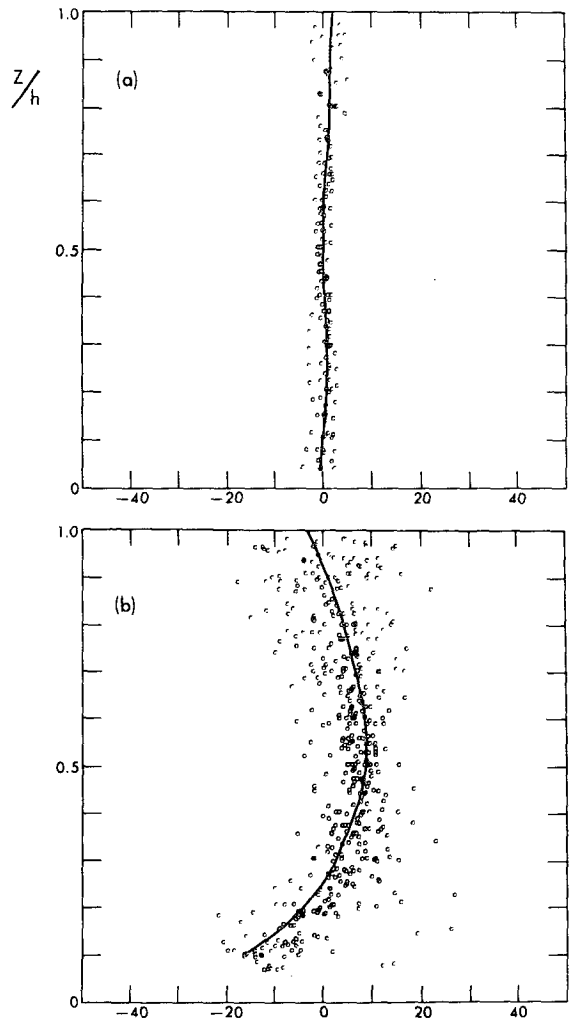

Fig 11 shows the relation between the nondimensional height scales h/L and $u_*/|f|L$. An expression $h/L=0.3u_*|f|L$ seems to hold near neutral stability ($|h/L|\leqslant 200$) but it underestimates h considerably when the stability takes values $|h/L|>200$. It is not immediately clear why h under strong stable conditions is considerably larger than $0.3u_*/|f|$. Previous investigators (e.g., Zilitinkevich, 1972; Businger and Arya, 1974) reported opposite results. The nighttime surface inversion layer (determined from Fig. 1) develops about an hour and a half before sunset and increases in height quickly with time at the beginning and levels off at later periods (Carson, 1973). Deepening of the surface inversion layer depends mainly on the heat transfer due to radiation, horizontal transport and turbulence mixing. Since the authors cited above included only the atmospheric cooling due to turbulence mixing, their surface inversion layer height might be underestimated considerably. More recent work by Yamada and Mellor (1975) found that the cooling due to radiation and horizontal transport were dominant during the nighttime but their h's were again found much smaller than $0.3u_*/|f|$. Therefore the result $h>0.3u_*/|f|$ as indicated in Fig. 11 under strong stable conditions appears to be contradictory to the results obtained by numerical models in which the heat transfer due to radiation, horizontal transport and turbulence mixing might not have been properly treated. On the other hand, the surface inversion layer height from the virtual potential temperature profile can be by no means determined precisely. The similarity functions

A, B and C will be affected by the errors in h much more strongly under stable conditions than under unstable conditions.[5]

b. *Predictions of C_D, C_H and θ*

The drag coefficient, the heat transfer coefficient, and the surface wind angle may be predicted from (5a), (5b) and (6) when the similarity functions A, B and C are expressed in terms of the stability parameter h/L. The solid lines in Figs. 2–4 are determined in such a way that the resultant similarity functions A, B and C would predict realistically the drag coefficient, the heat transfer coefficient, and the surface wind angle deduced from the present data set. The data values are calculated from $C_D \equiv u_*/|\hat{\mathbf{V}}|$, $C_H \equiv T_*/(\hat{\Theta}_v - \Theta_{v0})$ and $\theta \equiv \tan^{-1}(\hat{V}/\hat{U})$ and presented in Figs. 12–14 as a function of the bulk Richardson number

[5] The writer of this paper is grateful to the reviewer who brought his attention to this subject.

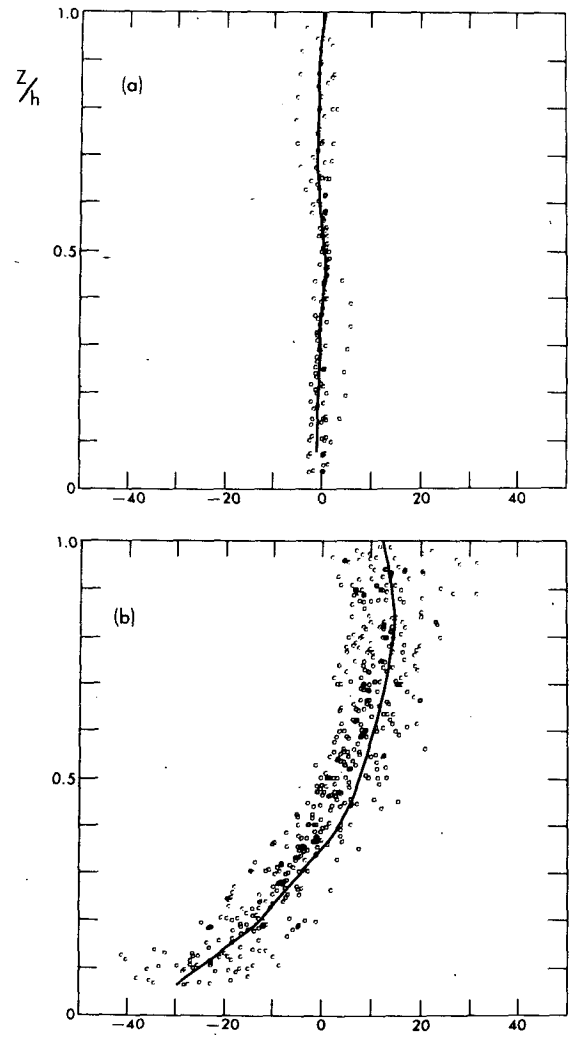

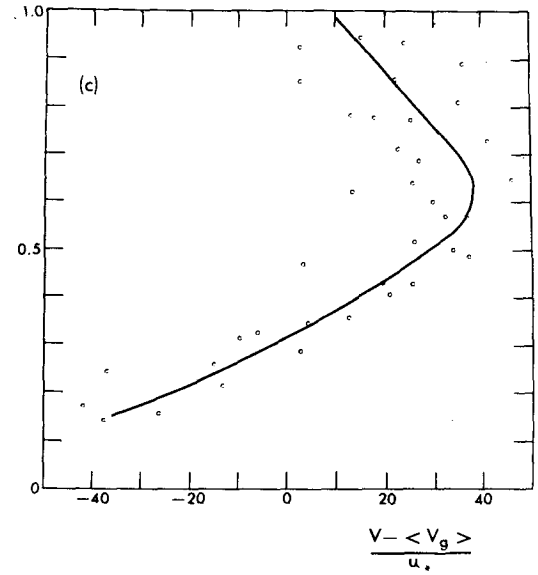

FIG. 16. As in Fig. 15 except for $(V-\langle V_g\rangle)/u_*$.

defined as

$$\mathrm{Ri}_B \equiv \frac{\beta g h(\hat{\Theta}_v - \Theta_{v0})}{|\hat{\mathbf{V}}|^2} = \mathrm{Pr}_0 \frac{h}{L} \frac{\ln(h/z_0) - C}{\{[\ln(h/z_0) - A]^2 + B^2\}}. \quad (12)$$

This is the same expression as in Melgarejo and Deardorff (1974) (except that A and B are switched). The second equality in (12) is obtained from (5a) and (5b).

The values for the similarity functions A, B and C at the neutral stability condition ($\mathrm{Ri}_B = h/L = 0$) are first determined as follows. From (5a) and (6) we obtain $B = k \sin\theta / C_D$. The average values for θ and C_D at $\mathrm{Ri}_B = 0$ may be obtained as 15° and 0.03 from Figs. 12 and 14, respectively. Utilizing these values we obtain $B = 3.020$. Then Eq. (5a) gives $A = 1.855$ for $h/z_0 = 5 \times 10^5$ which is the average value obtained from the present data set. Similarly the neutral value for C of 3.665 is obtained by substituting into (5b) the values $C_H = 0.05$ interpolated at $\mathrm{Ri}_B = 0$ from Fig. 13 and $h/z_0 = 5 \times 10^5$ as previously.

Under stable conditions Figs. 2–4 appear to suggest that the functions A, B and C decrease their gradients as the stability increases. Thus we assume a simple empirical expression, $Y = P + Qh/L$ for $0 \leqslant h/L \leqslant T$ and $Y = R(h/L + S)^{\frac{1}{3}}$ for $T < h/L$, where Y stands for either A, B or C and the numerical values for the constants P, Q, R, S and T must be determined empirically for each function of A, B and C. After several trials the following expressions for A, B and C are found to obtain the averaged data values in Figs. 2–4 and also realistically predict the data deduced drag coefficient, the heat transfer coefficient and the

surface wind angle as shown in Figs. 12–14:

$$A=\begin{cases}1.855-0.380h/L & \text{for } 0\leqslant h/L\leqslant 35 \quad (13a)\\ -2.94(h/L-19.94)^{\frac{1}{2}} & \text{for } 35<h/L \quad (13b)\end{cases}$$

$$B=\begin{cases}3.020+0.300h/L & \text{for } 0\leqslant h/L\leqslant 35 \quad (14a)\\ 2.85(h/L-12.47)^{\frac{1}{2}} & \text{for } 35<h/L \quad (14b)\end{cases}$$

$$C=\begin{cases}3.665-0.829h/L & \text{for } 0\leqslant h/L\leqslant 18 \quad (15a)\\ -4.32(h/L-11.21)^{\frac{1}{2}} & \text{for } 18<h/L. \quad (15b)\end{cases}$$

On the other hand, under unstable conditions, Figs. 2–4 appear to indicate that the similarity functions approach constant values as the instability increases. We simply assume an expression in a form $Y'=P'+Q'(1-R'h/L)^{-\frac{1}{3}}$, where Y' stands for either A, B or C and the constants P', Q' and R' are determined in a similar fashion as described under stable conditions. The final expressions obtained for A, B and C under unstable conditions are

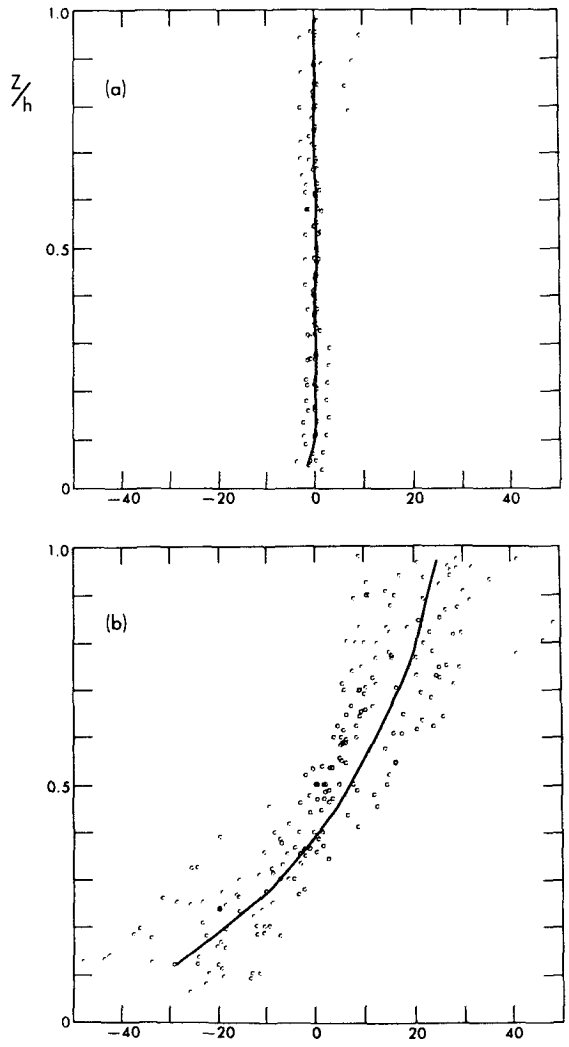

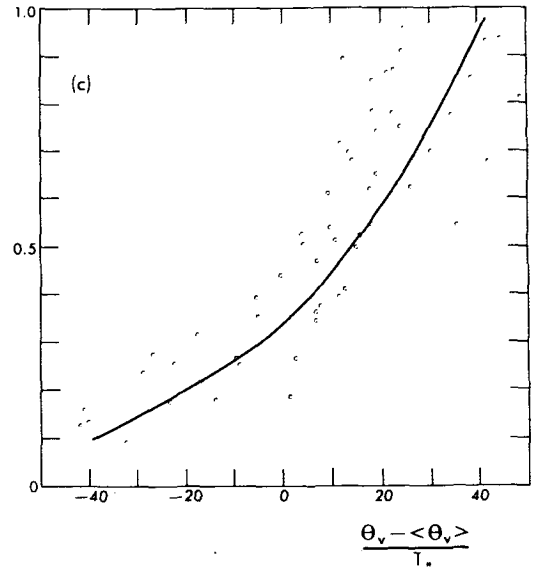

FIG. 17. Temperature defect $(\Theta_v-\langle\Theta_v\rangle)/T_*$ (abscissa) vs z/h (ordinate): (a) $-60\leqslant h/L\leqslant -30$; (b) $0\leqslant h/L\leqslant 30$; (c) $60\leqslant h/L\leqslant 90$.

$$A=10.0-8.145(1.0-0.008376\ h/L)^{-\frac{1}{3}}, \quad (16)$$

$$B=3.020(1.0-3.290\ h/L)^{-\frac{1}{3}}, \quad (17)$$

$$C=12.0-8.335(1.0-0.03106\ h/L)^{-\frac{1}{3}}. \quad (18)$$

The graphical presentations of A, B and C are included in Figs. 2, 3 and 4, respectively.

c. *Universalities in the wind and temperature profiles*

A direct validity test for the similarity profile functions for wind and virtual potential temperature are conducted according to Eqs. (1a)–(1c) which state that wind and temperature profiles, under a fixed stability condition, must obey the corresponding universal function. Since the number of runs at any fixed h/L values is small several runs are grouped into one stability class as indicated in Figs. 15–17. Although scatter around the curves fitted to the data is large, distinct differences for different stability classes are in evidence. For example, very uniform wind profiles exist under unstable conditions, but maxima are clearly seen in the profiles under strong stable conditions.

5. Summary and remarks

Various scales of the similarity theory are tested by examining the universalities of the similarity functions A, B and C which are computed from the Wangara atmospheric data. Minimum scatter in A, B and C is obtained when vertically averaged geostrophic wind and mean virtual potential temperature, suggested by Arya and Wyngaard (1975), are utilized as

the wind and temperature scales together with the height scale h which is taken as the height of the mixed layer during the day but as the height of the surface inversion layer during the night. The second best results are obtained when the local wind and virtual potential temperature at h are utilized in place of the vertically averaged values of the corresponding variables. Finally, slightly more scatter is found under stable conditions when a more conventional height scale $u_*/|f|$ replaced h, which agrees with the findings by Melgarejo and Deardorff (1974). Under unstable conditions the similarity functions A, B and C showed relatively small variations for all scales tested here but order of superiority of one scale over another still leads to the same conclusion as that found under stable conditions.

Although noticeable improvements over the results previously reported are achieved by utilizing the present scales no claim is made that the present similarity functions A, B and C have satisfactorily demonstrated universalities as the theory requires. As found by previous investigators, scattering in A, B and C appears to increase with increasing stability. Part of the variations are believed to be caused by the errors in evaluating the surface heat and momentum fluxes. Friction velocity and surface heat fluxes were not obtained from direct measurements but were inferred from the observed wind and temperature profiles and by the similar procedure described by Paulson (1970). In order to test the validity of such procedures the computed heat fluxes are compared with the direct measurements taken during the afternoons of Day 26 through Day 31 of the Wangara experiment. The results are shown in Fig. 18 (see Appendix B for details) which partially explains the scatter in the similarity functions A, B and C under unstable conditions. No such tests are conducted under stable conditions since no direct measurements of the turbulent surface fluxes are reported in the Wangara experiment.

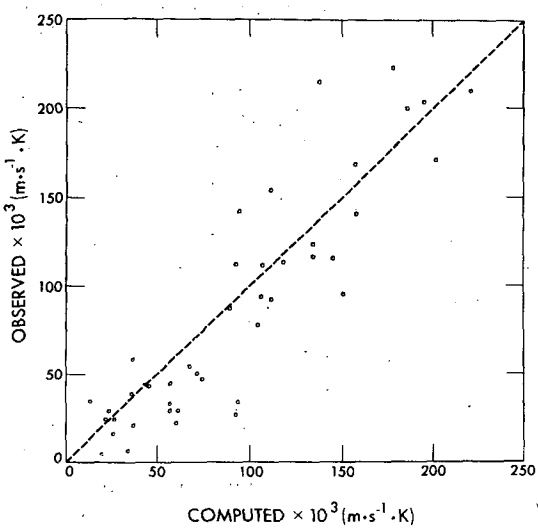

FIG. 18. Comparison of observed and computed surface heat fluxes.

An additional attempt is made to include the effect of nonstationarity in evaluation of the mean geostrophic wind, i.e., the tendency terms are retained in the mean equation of motion (9a,b), after which integration of these equations yields

$$\langle U_g\rangle = \langle U\rangle + \frac{1}{|f|}\frac{\partial}{\partial t}\langle V\rangle \operatorname{sign} f,$$

$$\langle V_g\rangle = \langle V\rangle - \frac{u_*^2}{|f|h}\operatorname{sign} f - \frac{1}{|f|}\frac{\partial}{\partial t}\langle U\rangle \operatorname{sign} f.$$

Unfortunately, this set of the wind scales resulted in more scatter in A, B and C than that without the correction of the tendency terms. It is believed that large errors could be introduced in evaluating the time derivatives of the winds from the data which are available only hourly.

Acknowledgments. The author is grateful to Dr. A. E. Gill for reading the manuscript and for valuable suggestions. Mr. B. Hicks of Argonne National Laboratory confirmed the temperature errors in the Wangara report due to the malfunction of the temperature sensor and suggested using the temperature difference between 1 and 4 m as discussed in the text. Discussions with Dr. D. Hess of Argonne National Laboratory and Prof. G. Mellor of Princeton University are appreciated. His thanks also go to Mr. T. Dickey for editing, Mmes. C. Longmuir and E. Olsen for typing the manuscript, and to Mr. P. Tunison for drafting the figures.

APPENDIX A

List of Symbols

A, B, C	similarity functions defined by Eqs. (4a)–(4c)
C_D, C_H	drag and heat transfer coefficients defined by (5a) and (5b), respectively.
$F_u, F_v, F_{\Theta_v}, \mathbf{F}$	universal outer (profile) functions for $(U, V, \Theta_v, \mathbf{V})$
H_0	surface heat flux $[\equiv(-\overline{\omega\theta})_0]$
L	Obukhov length $[\equiv u_*^3/(k\beta g H_0)]$
Pr_0	turbulent Prandtl number at the neutral stability (0.74 according to Businger *et al.*, 1971)
R	mixing ratio of water vapor
Ri_B	bulk Richardson number defined by (12)
T	absolute temperature
T_v	virtual temperature $[=T(1+0.61R)]$
T_*	friction temperature $[=H_0/u_*]$
U, V	wind components tangential and normal to the surface stress direction

$\mathbf{V}$	wind vector $[=U\cdot\mathbf{t}+V\cdot\mathbf{n}]$
$\hat{U}, \hat{V}, \hat{\mathbf{V}}$	Wind scales for $(U, V, \mathbf{V})$
$\lvert\hat{\mathbf{V}}\rvert$	$[=(\hat{U}^2+\hat{V}^2)^{\frac{1}{2}}]$
U_g, V_g	geostrophic wind components tangential and normal to the surface stress direction
$\mathbf{V}_g$	$[=U_g\cdot\mathbf{t}+V_g\cdot\mathbf{n}]$
f	Coriolis parameter
g	acceleration of gravity
h	height scale
u_*	friction velocity
$\mathbf{n}, \mathbf{t}$	unit vectors normal and tangential to the surface stress direction
z	vertical coordinate
z_0	roughness height
Θ_v	virtual potential temperature
Θ_{v0}	Θ_v at $z=z_0$
$\hat{\Theta}_v$	temperature scale
β	thermal expansion coefficient
γ_d	dry adiabatic lapse rate [10 K (1000 m)$^{-1}$]
k	von Kármán constant [=0.35 according to Businger *et al.* (1971)]
ψ_m, ψ_h	stability functions for wind and temperature
θ	angle between the surface stress and that of $\hat{\mathbf{V}}=\hat{U}\cdot\mathbf{t}+\hat{V}\cdot\mathbf{n}$
$\langle\eta\rangle$	verticaly averaged value of η

$$\left[\equiv\frac{1}{h}\int_{z_0}^{h}\eta dz\right]$$

APPENDIX B

Remarks on the Determination of the Surface Fluxes using the Empirical Formulas

As noted in the text a reviewer of this paper pointed out that the temperature differences between 1 and 2 m reported in Clarke *et al.* (1971) were in error due to the malfunction of the temperature sensor at 2 m above the surface (Hicks, 1975). The present author had calculated the surface fluxes by using the temperature difference between 1 and 2 m in the original manuscript and compared these calculated values with the direct measurements taken during the afternoons of Days 26 through 31 of the Wangara experiment. After receiving the reviewer's comment the same calculation was repeated but using the temperature difference at 1 and 4 m. The results are very much improved. In order to assess the degree of improvement quantitatively, the following "indicators" were computed:

$$\sigma_1^2=\frac{1}{N}\sum_{i=1}^{N}[(H_{\rm obs})_i-(H_{\rm cal})_i]^2, \qquad \text{(B1)}$$

$$\sigma_2^2=\frac{1}{N}\sum_{i=1}^{N}[1.0-(H_{\rm cal})_i/(H_{\rm obs})_i]^2, \qquad \text{(B2)}$$

where $H_{\rm obs}$ and $H_{\rm cal}$ are observed and calculated heat fluxes, respectively; N is the total number of cases which was 43; and σ_1 may approximately correspond to the standard deviation and σ_2 may be interpreted as a weighted value of σ_1. Fig. 18 shows a comparison of the observed and calculated surface heat fluxes where the Businger *et al.* formula (1971) and the temperature difference at 1 and 4 m were used. The indicators σ_1 and σ_2 for this case were 1.016 and 0.02873, respectively. If the temperature differences at 1 and 2 m were used, the corresponding values for σ_1 and σ_2 increased to 1.6545 and 0.03818, respectively. A plot similar to Fig. 18 (not shown here) for the latter case clearly indicated poorer correlations, than the former case, between the observed and computed surface heat fluxes. If wind and temperature differences at 1 and 4 m were used we obtained $\sigma_1=1.157$ and $\sigma_2=0.0337$. All the calculations mentioned above were based on the empirical formulas for ϕ_m and ϕ_h by Businger *et al.* (1971). Different but equally valid formulas are available (Dyer, 1974), among which the formulas given by Dyer and Hicks (1970) were utilized to repeat the surface heat flux calculations. The results are given in Table 1, from which we found that the formulas by Businger *et al.* with the temperature difference between 1 and 4 m and wind at 0.5 m above the surface gave the best performance. Equally valid results were obtained if the formulas in Dyer and Hicks were utilized together with the temperature and wind differences at 1 and 4 m.

All the results presented in the text are based on the surface fluxes obtained by the formulas by Businger *et al.* (1971) with the temperature difference between 1 and 4 m and the wind at 0.5 m above the surface. The computed surface properties are summarized in Table 2.

TABLE 1. Performance of the empirical wind and temperature formulas. B and DH indicates the empirical formulas by Businger *et al.* (1971) and Dyer and Hicks (1970), respectively. Subscripts represent the height (m) above the ground; σ_1 and σ_2 are defined by (B1) and (B2).

	Temperature	Wind	σ_1	σ_2
B	T_4-T_1	$U_{0.5}$	1.016	0.0287
B	T_2-T_1	$U_{0.5}$	1.655	0.0382
DH	T_4-T_1	$U_{0.5}$	1.105	0.0332
DH	T_2-T_1	$U_{0.5}$	1.775	0.0456
B	T_4-T_1	U_4-U_1	1.157	0.0337
DH	T_4-T_1	U_4-U_1	1.082	0.0293

TABLE 2. u_*, T_*, H_0 and L determined for the Wangara experiment.

Day	Hour	L (m)	u_* (ms)	T_* (K)	H_0 (mKs)
		stable conditions			
1	6	3.1	0.047	0.0588	-0.0028
	21	8.2	0.094	0.0880	-0.0082
2	0	25.4	0.168	0.0908	-0.0153
4	3	14.2	0.117	0.0796	-0.0094
	6	24.3	0.191	0.1221	-0.0233
6	21	4.1	0.066	0.0878	-0.0058
7	3	2.9	0.050	0.0704	-0.0035
	6	4.4	0.063	0.0723	-0.0045
	21	1.5	0.042	0.0876	-0.0035
8	0	3.9	0.069	0.0999	-0.0069
11	3	12.4	0.082	0.0438	-0.0036
	4	17.8	0.104	0.0501	-0.0052
	5	29.3	0.116	0.0372	-0.0043
	6	28.1	0.101	0.0298	-0.0030
	21	14.4	0.126	0.0907	-0.0114
	22	14.9	0.124	0.0851	-0.0106
	23	11.8	0.102	0.0724	-0.0074
12	0	21.3	0.151	0.0871	-0.0131
	1	17.0	0.124	0.0736	-0.0091
	2	18.1	0.138	0.0853	-0.0118
	5	24.4	0.158	0.0830	-0.0131
	6	29.9	0.171	0.0794	-0.0136
	21	13.2	0.111	0.0768	-0.0085
	22	15.8	0.125	0.0803	-0.0100
	23	12.0	0.103	0.0717	-0.0074
13	0	13.5	0.109	0.0711	-0.0077
	1	20.1	0.153	0.0951	-0.0146
	2	10.0	0.110	0.0989	-0.0109
	3	7.8	0.101	0.1064	-0.0108
	4	4.8	0.062	0.0544	-0.0040
	5	6.7	0.079	0.0750	-0.0059
	6	7.8	0.090	0.0828	-0.0074
	21	4.7	0.072	0.0897	-0.0064
	22	3.1	0.053	0.0751	-0.0040
	23	4.7	0.071	0.0871	-0.0062
14	0	4.6	0.068	0.0817	-0.0056
	1	8.1	0.096	0.0920	-0.0088
	2	8.0	0.093	0.0869	-0.0081
	3	11.6	0.120	0.0998	-0.0119
	4	4.9	0.069	0.0790	-0.0055
	5	4.3	0.062	0.0715	-0.0044
	6	12.7	0.135	0.1162	-0.0156
	21	3.0	0.050	0.0701	-0.0035
	22	1.5	0.030	0.0468	-0.0014
	23	2.5	0.047	0.0723	-0.0034
19	0	21.9	0.166	0.1027	-0.0171
	3	14.9	0.124	0.0834	-0.0104
	6	15.7	0.121	0.0747	-0.0091
26	6	6.3	0.056	0.0409	-0.0023
	21	6.4	0.071	0.0659	-0.0047
30	21	20.8	0.154	0.0924	-0.0142
31	0	38.1	0.204	0.0853	-0.0171
	1	32.5	0.187	0.0863	-0.0161
	2	38.0	0.204	0.0877	-0.0179
	3	21.5	0.146	0.0791	-0.0115
	4	24.9	0.159	0.0814	-0.0130
	5	27.1	0.164	0.0793	-0.0130
	6	20.2	0.135	0.0730	-0.0099
	21	2.8	0.050	0.0721	-0.0036
	22	3.0	0.047	0.0606	-0.0029
	23	4.4	0.061	0.0692	-0.0042
32	0	7.5	0.077	0.0628	-0.0048
	1	15.0	0.113	0.0678	-0.0076
	2	4.7	0.062	0.0665	-0.0041
	3	4.6	0.050	0.0433	-0.0022
	4	1.1	0.021	0.0319	-0.0007
	5	0.9	0.019	0.0335	-0.0007
	6	2.5	0.044	0.0613	-0.0027
	21	6.2	0.069	0.0623	-0.0043
	22	4.7	0.062	0.0657	-0.0040
	23	2.9	0.044	0.0534	-0.0024
33	0	3.3	0.053	0.0675	-0.0036
	1	4.2	0.062	0.0736	-0.0046
	2	7.6	0.088	0.0814	-0.0071
	3	7.2	0.081	0.0728	-0.0059
	4	6.4	0.065	0.0520	-0.0034
	5	1.5	0.019	0.0190	-0.0004
	6	0.4	0.006	0.0062	-0.0000
	21	3.9	0.063	0.0825	-0.0052
	22	2.4	0.044	0.0630	-0.0027
	23	3.9	0.065	0.0890	-0.0058
34	0	5.0	0.070	0.0805	-0.0057
	1	4.0	0.062	0.0760	-0.0047
	2	3.9	0.063	0.0803	-0.0050
	3	4.6	0.073	0.0934	-0.0068
	4	3.3	0.053	0.0700	-0.0037
	5	4.0	0.066	0.0863	-0.0057
	6	16.3	0.134	0.0887	-0.0119
	21	6.6	0.089	0.0991	-0.0083
	22	5.8	0.085	0.1016	-0.0087
35	3	52.4	0.279	0.1216	-0.0339
	4	53.4	0.282	0.1221	-0.0345
	5	75.9	0.339	0.1242	-0.0422
	6	35.6	0.224	0.1157	-0.0260
	21	94.0	0.302	0.0804	-0.0242
36	0	112.4	0.346	0.0882	-0.0305
	1	105.3	0.356	0.0996	-0.0354
	2	107.0	0.353	0.0968	-0.0342
	3	82.4	0.300	0.0906	-0.0272
	4	98.5	0.332	0.0928	-0.0308
36	5	58.4	0.261	0.0967	-0.0252
	21	21.2	0.128	0.0641	-0.0082
	22	17.0	0.119	0.0680	-0.0081
	23	7.5	0.078	0.0674	-0.0053
37	0	10.4	0.101	0.0796	-0.0080
	1	9.0	0.087	0.0687	-0.0060
	2	8.1	0.074	0.0545	-0.0040
	3	20.1	0.087	0.0304	-0.0026
	4	23.2	0.123	0.0536	-0.0066
	5	14.0	0.099	0.0569	-0.0056
	6	35.9	0.127	0.0370	-0.0047
	21	31.8	0.163	0.0691	-0.0112
	22	26.0	0.145	0.0669	-0.0097
	23	31.5	0.178	0.0831	-0.0148
38	0	32.8	0.170	0.0721	-0.0122
	1	28.6	0.188	0.1014	-0.0190
	2	39.8	0.195	0.0786	-0.0154
	3	39.6	0.192	0.0760	-0.0146
	4	42.2	0.206	0.0824	-0.0170
	5	45.9	0.204	0.0735	-0.0150
	6	28.9	0.155	0.0671	-0.0104
	21	51.7	0.209	0.0701	-0.0146
	22	58.7	0.221	0.0691	-0.0153
	23	32.1	0.188	0.0908	-0.0171
39	3	19.0	0.132	0.0753	-0.0100
42	21	3.8	0.062	0.0830	-0.0051
43	0	4.8	0.065	0.0734	-0.0048
	3	16.7	0.156	0.1199	-0.0187
44	3	69.3	0.278	0.0911	-0.0253
	6	64.2	0.282	0.1012	-0.0285
		unstable conditions			
7	12	-13.6	0.231	-0.3284	0.0760
	15	-10.7	0.171	-0.2293	0.0391
11	10	-34.1	0.262	-0.1655	0.0434
	12	-19.5	0.286	-0.3470	0.0992
	13	-23.0	0.295	-0.3161	0.0934
	15	-30.7	0.258	-0.1816	0.0469
12	10	-56.0	0.254	-0.0947	0.0240
	11	-33.2	0.262	-0.1705	0.0446
	12	-15.5	0.252	-0.3422	0.0863
	13	-16.8	0.269	-0.3599	0.0968
	14	-32.4	0.269	-0.1884	0.0507
	15	-21.7	0.242	-0.2273	0.0550
13	10	-28.6	0.283	-0.2322	0.0657
	11	-23.0	0.293	-0.3115	0.0913
	12	-28.7	0.328	-0.3152	0.1034
	13	-12.8	0.246	-0.3982	0.0979
	14	-10.5	0.232	-0.4339	0.1006
	15	-19.3	0.276	-0.3338	0.0921
14	10	-39.3	0.269	-0.1534	0.0413
	11	-16.1	0.230	-0.2741	0.0631
	12	-10.1	0.223	-0.4097	0.0912
	13	-6.4	0.185	-0.4514	0.0837
	14	-4.4	0.165	-0.5202	0.0657
	15	-5.6	0.160	-0.3830	0.0611
26	12	-39.7	0.258	-0.1408	0.0363
	15	-44.8	0.218	-0.0894	0.0195
31	10	-20.9	0.306	-0.3649	0.1116
	11	-13.5	0.296	-0.5334	0.1578
	12	-10.9	0.291	-0.6393	0.1861
	13	-6.9	0.261	-0.8220	0.2149
	14	-10.5	0.257	-0.5233	0.1347
	15	-12.4	0.242	-0.3906	0.0944
32	10	-11.3	0.225	-0.3690	0.0830
	11	-7.4	0.221	-0.5421	0.1196
	12	-4.1	0.188	-0.7134	0.1344
	13	-3.0	0.168	-0.7891	0.1327
	14	-2.3	0.160	-0.9196	0.1468
	15	-4.5	0.180	-0.6079	0.1097
33	10	-1.4	0.135	-1.0764	0.1458
	11	-1.3	0.125	-1.0376	0.1300
	12	-1.3	0.143	-1.2825	0.1835
	13	-0.7	0.113	-1.4975	0.1689
	14	-2.0	0.158	-1.0294	0.1623
	15	-2.1	0.155	-0.9623	0.1490
34	10	-17.9	0.279	-0.3591	0.1000
	11	-18.9	0.313	-0.4314	0.1349
	12	-15.2	0.301	-0.5012	0.1510
	13	-12.4	0.281	-0.5356	0.1505
	14	-13.6	0.292	-0.5327	0.1557

TABLE 2. *Continued* (unstable conditions)

Day	Hour	L (m)	u_* (ms)	T_* (K)	H_0 (mKs)
	15	-14.0	0.284	-0.4860	0.1382
35	10	-57.9	0.438	-0.2750	0.1204
	11	-54.1	0.441	-0.3011	0.1329
	12	-42.1	0.418	-0.3487	0.1456
	13	-29.2	0.404	-0.4714	0.1903
	14	-34.0	0.382	-0.3651	0.1395
	15	-67.1	0.363	-0.1661	0.0503
36	10	-81.3	0.304	-0.0947	0.0288
	13	-14.2	0.247	-0.3611	0.0890
	14	-18.1	0.201	-0.1889	0.0379
	15	-24.6	0.205	-0.1445	0.0297
37	10	-34.6	0.140	-0.0466	0.0065
	12	-66.3	0.200	-0.0503	0.0101
	13	-102.5	0.234	-0.0445	0.0106
	14	-1071.6	0.211	-0.0034	0.0007
	15	-172.2	0.193	-0.0180	0.0035
38	10	-38.7	0.330	-0.2327	0.0768
	11	-43.1	0.385	-0.2861	0.1101
	14	-91.2	0.356	-0.1163	0.0414
	15	-134.3	0.359	-0.0802	0.0288

REFERENCES

Arya, S. P. S., 1975: Geostrophic drag and heat transfer relations for the atmospheric boundary layer. *Quart. J. Roy. Meteor. Soc.*, **101**, 147–161.

——, and J. C. Wyngaard, 1975: Effect of baroclinicity on wind profiles and the geostrophic drag law for the convective planetary boundary layer. *J. Atmos. Sci.*, **32**, 767–778.

Blackadar, A. K., and H. Tennekes, 1968: Asymptotic similarity in neutral barotropic planetary boundary layers. *J. Atmos. Sci.*, **25**, 1015–1020.

Brown, R. A., 1974: Matching classical boundary-layer solutions toward a geostrophic drag coefficient relation. *Bound.-Layer Meteor.*, **7**, 489–500.

Businger, J. A., and S. P. S. Arya, 1974: Height of the mixed layer in the stably stratified planetary boundary layer. *Advances in Geophysics*, Vol. 18A, Academic Press, 73-92.

——, J. C. Wyngaard, Y. Izumi and E. F. Bradley, 1971: Flux profile relationships in the atmospheric surface layer. *J. Atmos. Sci.*, **28**, 181–189.

Carson, D. J., 1973: The development of a dry inversion-capped convectively unstable boundary layer. *Quart. J. Roy. Meteor. Soc.*, **99**, 450–467.

Clarke, R. H., 1970a: Recommended methods for the treatment of the boundary layer in numerical models *Aust. Meteor. Mag.*, **28**, 51–73.

——, 1970b: Observational studies in the atmospheric boundary layer. *Quart. J. Roy. Meteor. Soc.*, **96**, 91–114.

——, and G. D. Hess, 1973: On the appropriate scaling for velocity and temperature in the planetary boundary layer. *J. Atmos. Sci.*, **30**, 1346–1353.

——, and ——, 1974: Geostrophic departure and the functions A and B of Rossby-number similarity theory. *Bound.-Layer Meteor.*, **7**, 267–287.

——, A. J. Dyer, R. R. Brook, D. G. Reid and A. J. Troup, 1971: The Wangana experiment: Boundary layer data. Tech. paper 19, Div. Meteor. Phys., CSIRO, Australia.

Csanady, G. T., 1967: On the resistance law of a turbulent Ekman Layer. *J. Atmos. Sci.*, **24**, 467–471.

——, 1972: Geostrophic drag, heat and mass transfer coefficients for the diabatic Ekman layer. *J. Atmos. Sci.*, **29**, 488–496.

Deardorff, J. W., 1972: Numerical investigation of neutral and unstable planetary boundary layer. *J. Atmos. Sci.*, **29**, 91–115.

——, 1973: An explanation of anomalously large Reynolds stresses within the convective planetary boundary layer. *J. Atmos. Sci.*, **30**, 1070–1076.

Dyer, A. J., 1974: A review of flux-profile relations. *Bound.-Layer Meteor.*, **1**, 363–372.

——, and B. B. Hicks, 1970: Flux-gradient relationships in the constant flux layer. *Quart. J. Roy. Meteor. Soc.*, **96**, 715–721.

Gill, A. E., 1968: Similarity theory and geostrophic adjustment. *Quart. J. Roy. Meteor. Soc.*, **94**, 581–585.

Hess, G. D., 1973: On Rossby-number similarity theory for a baroclinic boundary layer. *J. Atmos. Sci.*, **30**, 1722–1723.

Hicks, B. B., 1975: Wind profile relationships from the "Wangara" experiment. (Submitted to the *Quart. J. Roy. Meteor. Soc.*)

Kazanski, A. B., and A. S. Monin, 1960: A turbulent regime above the surface atmospheric layer. *Izv. Acad. Sci.*, USSR, Geophys. Ser., No. 1, 110–112.

Melgarejo, J. W., and J. W. Deardorff, 1974: Stability functions for the boundary-layer resistance laws based upon observed boundary layer height. *J. Atmos. Sci.*, **31**, 1324–1333.

——, and ——, 1975: Revision to "Stability functions for the boundary-layer resistance laws based upon observed boundary layer heights." *J. Atmos. Sci.*, **32**, 837–839.

Paulson, C. A., 1970: The mathematical representation of wind speed and temperature profiles in the unstable atmospheric surface layer. *J. Appl. Meteor.*, **9**, 857–861.

Wyngaard, J. C., O. R. Coté and K. S. Rao, 1974: Modeling the atmospheric boundary layer. *Advances in Geophysics*, Vol. 18A, Academic Press, 193–211.

Yamada, T., and G. L. Mellor, 1975: A simulation of the Wangara atmospheric boundary layer data. *J. Atmos. Sci.*, **32**, 2309–2329.

Zilitinkevich, S. S., 1972: On the determination of the height of the Ekman boundary layer. *Bound.-Layer Meteor.*, **3**, 141–145.

——, 1975: Resistance laws and prediction equations for the depth of the planetary boundary layer. *J. Atmos. Sci.*, **32**, 741–752.

——, and D. V. Chalikov, 1968: The laws of resistance and of heat and moisture exchange in the interaction between the atmosphere and an underlying surface. *Izv. Atmos. Oceanic Phys.*, 4, 438–441.

——, D. L. Laikhtman and A. S. Monin, 1967: Dynamics of the atmospheric boundary layer. *Izv. Atmos. Oceanic Phys.*, **3**, 170–191.